

# USING DYNAMIC INDICATORS FOR PROBING SINGLE-PARTICLE STABILITY IN CIRCULAR ACCELERATORS\*

C.E. Montanari<sup>1</sup>, A. Bazzani, G. Turchetti, Bologna University, Bologna, Italy  
M. Giovannozzi, CERN Beams Department, Geneva, Switzerland  
<sup>1</sup>also at CERN Beams Department, Geneva, Switzerland

## Abstract

Computing the long-term behaviour of single-particle motion is a numerically expensive process, as it requires a large number of initial conditions to be tracked for a large number of turns to probe their stability. A possibility to reduce the computational resources required is to provide indicators that can efficiently detect the chaotic character of the orbits, which is considered a precursor of unbounded motion. These indicators could allow skilful selection of sets of initial conditions that are then considered for long-term tracking. The chaotic nature of each orbit can be assessed by using fast-converging dynamic indicators, such as the Fast Lyapunov Indicator (FLI), the Reversibility Error Method (REM), and the Smallest and Global Alignment Index (SALI and GALI). These indicators are widely used in the field of celestial mechanics, but not so widespread in accelerator physics. We have studied their efficiency by applying them both to a modulated Hénon map, as a toy model, and to realistic lattices of the High-Luminosity LHC. In this paper, we discuss the results of detailed numerical studies, focusing on their performance in detecting chaotic motions.

## INTRODUCTION

The chaotic character of the orbits of a Hamiltonian system, such as the  $4d$  modulated Hénon map [1], which describes the transverse motion in a circular accelerator [2] or a realistic accelerator lattice such as that of the HL-LHC [3], can be analysed by means of dynamic indicators. These are quantities that probe the linear response to an initial small random displacement or to random displacements along the orbit. Dynamic indicators have been one of the main tools for studying the chaotic character and long-term stability in many specific problems in celestial mechanics [4–6].

As direct tracking of realistic accelerator lattices on timescales of physical interest, i.e.  $10^8$  turns, is not an option for several initial conditions, there is a strong interest in tools that can probe the long-term behaviour of initial conditions at lower numbers of turns. Well-established dynamic indicators, like the Fast Lyapunov Indicator (FLI) [6], have been applied to accelerator physics, together with indicators based on harmonic analysis [7]. Recently, studies based on the Reversibility Error Method (REM) [5] have also been performed [8]. However, modern dynamic indicators such as the Smallest and Global Alignment Index (SALI and GALI) [9] have not yet been extensively considered in accelerator studies. Moreover, a general overview

of different dynamic indicators in accelerator models is not available. The study presented here is a first step in assessing the performance of these indicators for accelerator-related studies.

## OVERVIEW OF DYNAMIC INDICATORS

### Lyapunov-based Dynamic Indicators

Given a non-autonomous Hamiltonian map  $M(\mathbf{x}, n)$  in  $\mathbb{R}^{2d}$ ,  $DM(\mathbf{x}, n)$  denotes the symplectic Jacobian matrix  $(DM)_{ij} = \partial M_i / \partial x_j$  at the point  $\mathbf{x}$ , then the orbit of the map  $\mathbf{x}_n$  and the recurrence for the tangent map  $L_n$  are given by

$$\begin{aligned} \mathbf{x}_n &= M(\mathbf{x}_{n-1}, n-1) & \mathbf{x}_0 &= \mathbf{x} \\ L_n(\mathbf{x}) &= DM(\mathbf{x}_{n-1}, n-1) L_{n-1}(\mathbf{x}) & L_0 &= I. \end{aligned} \quad (1)$$

Note that in the autonomous case  $L_n(\mathbf{x}) = DM^{(n)}(\mathbf{x})$ . For any initial condition  $\mathbf{x}$  we consider a small stochastic deviation  $\epsilon \xi$ , where  $\xi$  is a random vector with zero mean and unit covariance matrix. Letting  $\mathbf{y}_n = M(\mathbf{y}_{n-1}, n-1)$  be the orbit with initial condition  $\mathbf{y}_0 = \mathbf{x} + \epsilon \xi$ , the linear response vector  $\Xi_n(\mathbf{x})$  is defined by

$$\Xi_n(\mathbf{x}) = \lim_{\epsilon \rightarrow 0} \frac{\mathbf{y}_n - \mathbf{x}_n}{\epsilon} = DM(\mathbf{x}_{n-1}, n-1) \Xi_{n-1}. \quad (2)$$

The FLI after  $n$  iterations is defined as  $FLI_n(\mathbf{x}) = \log \|\mathbf{L}_n(\mathbf{x}) \xi\| / n$ , and can be easily implemented with the ‘shadow particle’ method [10], i.e. estimating  $\|\mathbf{L}_n(\mathbf{x}) \xi\|$  by explicitly taking a companion particle with initial condition  $\mathbf{y}_0$  and computing the displacement after  $n$  turns, while performing norm renormalizations every  $m$  turns.

As FLI can be affected by the choice of  $\xi$  [11], a novel method consists in evaluating the eigenvalues and invariants of  $L_n L_n^T$  given by

$$L_n(\mathbf{x}) L_n^T(\mathbf{x}) = \langle \Xi_n(\mathbf{x}) \Xi_n^T(\mathbf{x}) \rangle \quad \text{with} \quad \langle \xi \xi^T \rangle = I. \quad (3)$$

This provides interesting results [12] as it is equivalent to considering all possible directions of the initial displacement vector. However, for complex maps, such as the Poincaré map of a realistic lattice, an analytical expression of the tangent map is not available, and the use of this method requires further considerations. A possible alternative is provided by the Orthogonal Fast Lyapunov Indicator (OFLI) [13], which consists in computing different FLI values along an orthonormal base of displacements. We refer to OFLI MAX as the maximum value obtained along the tracking and to OFLI MEAN as the mean of the computed values.

\* Research supported by the HL-LHC project

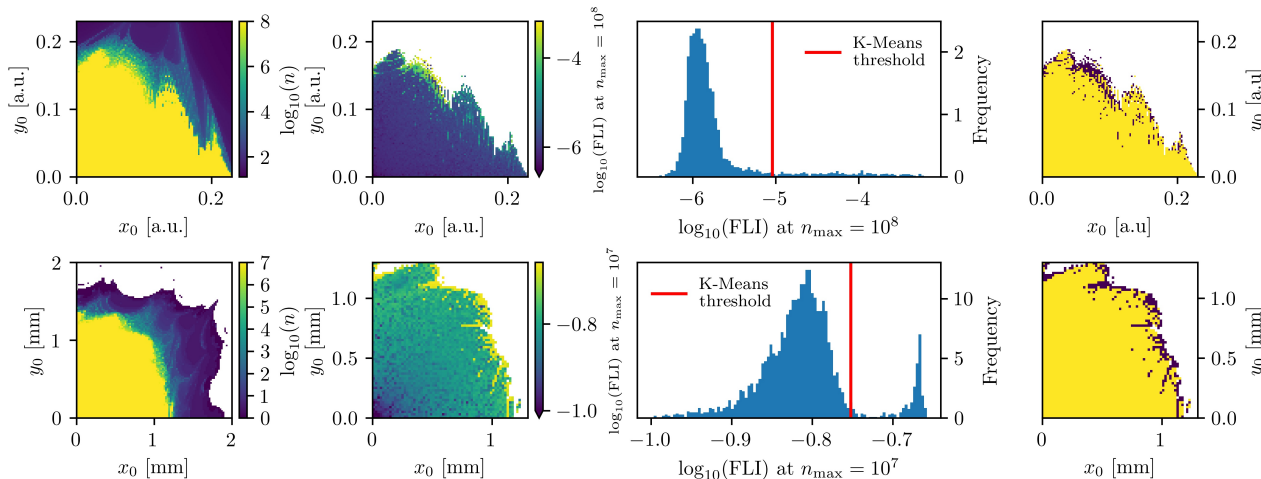


Figure 1: Ground Truth (GT) construction for the modulated Hénon-like map (top) and the HL-LHC (bottom). From left to right: a survival plot; FLI distribution for all initial conditions stable up to  $n_{\max}$ ; histogram of FLI values, clustered with a K-Means algorithm; binary classification of non-chaotic (yellow) and chaotic (purple) initial conditions.

### Reversibility Error Method

The REM is obtained from the linear response to a small stochastic deviation during  $n$  iterations of the map, followed by  $n$  iterations of the inverse map

$$\begin{aligned} \mathbf{y}_{n'} &= M(\mathbf{y}_{n'-1}, n' - 1) + \epsilon \xi_{n'} & 1 \leq n' \leq n \\ \mathbf{y}_{n'} &= M^{-1}(\mathbf{y}_{n'-1}, 2n - n') & n + 1 \leq n' \leq 2n. \end{aligned} \quad (4)$$

The linear response at iteration  $2n$  is given by

$$\Xi_{Rn}(\mathbf{x}) = \lim_{\epsilon \rightarrow 0} \frac{\mathbf{y}_{2n} - \mathbf{x}}{\epsilon} = \sum_{n'=1}^n L_{n'}^{-1} \xi_{n'}. \quad (5)$$

The round off produces a sort of pseudo-random deviation along the orbit, with amplitude  $\epsilon \sim 10^{-16}$ , in the 8 bytes standard IEEE754 [14] representation of reals. Since only one realisation is available, the absence of averaging results in significant fluctuations when  $n$  or  $\mathbf{x}$  are varied.

### SALI and GALI

SALI [15], and its generalisation GALI [16], are dynamic indicators based on the concept that linearly independent initial deviation vectors tend to coincide for chaotic motion when  $n \gg 1$ . The GALI order  $k$  indicators are given by the volumes of parallelotopes whose sides are the normalised images  $\xi_n^{(j)}$  of  $k$  linearly independent vectors  $\xi_j$  with  $1 \leq j \leq k$ , i.e.

$$\begin{aligned} \xi_n^{(j)}(\mathbf{x}) &= L_n(\mathbf{x}) \xi_j / \|L_n(\mathbf{x}) \xi_j\| \\ \text{GALI}_n^{(k)}(\mathbf{x}) &= \left\| \xi_n^{(1)}(\mathbf{x}) \wedge \dots \wedge \xi_n^{(k)}(\mathbf{x}) \right\|, \end{aligned} \quad (6)$$

and their asymptotic behaviour for chaotic orbits with  $k$  ordered positive Lyapunov exponents is given by

$$\text{GALI}_n^{(k)} \sim e^{-n[(\lambda_1 - \lambda_2) + \dots + (\lambda_{k-1} - \lambda_k)]}, \quad (7)$$

whereas for regular quasiperiodic orbits, whose Lyapunov exponents vanish, the GALI indicators decay as a power law. SALI is equivalent to GALI with  $k = 2$ , i.e. only 2 linearly independent deviation vectors are considered.

## RESULTS OF NUMERICAL SIMULATIONS

A 4d modulated Hénon-like map with octupolar kick [17], representing the Poincaré map of a FODO cell, has been used for the analysis of dynamic indicators. It reads

$$\begin{pmatrix} x' \\ p'_x \\ y' \\ p'_y \end{pmatrix}_{n+1} = R(\epsilon, n) \begin{pmatrix} x \\ p_x + x^2 - y^2 + \mu(x^3 - 3xy^2) \\ y \\ p_y - 2xy - \mu(3x^2y - y^3) \end{pmatrix}_n \quad (8)$$

where  $R(\epsilon, n)$  is the direct product of two  $2d$  rotations in the  $x - p_x$  and  $y - p_y$  planes, whose linear frequencies  $\omega_x(n)$  and  $\omega_y(n)$  vary with  $n$  according to

$$\omega_z(n) = \omega_{z0} \left( 1 + \epsilon \sum_{k=1}^m \epsilon_k \cos(\Omega_k n) \right) \quad z = x, y, \quad (9)$$

with  $\omega_{x0} = 0.31$ ,  $\omega_{y0} = 0.32$ . The harmonics  $\Omega_k$  are based on SPS measurements [1], along with relative amplitudes  $\epsilon_k$ , expressed in units of  $10^{-4}$ . Here, we consider the case with  $\epsilon = 16.0$  and  $\mu = 0.01$ , corresponding to a medium modulation strength and a weak octupolar kick.

The same analysis was performed for an HL-LHC [3] lattice, without beam-beam interaction, at 7.0 TeV, and tunes  $\omega_x = 0.31$ ,  $\omega_y = 0.32$ . All analyses performed for the HL-LHC lattice considered only the 4d transverse coordinates.

Single-particle tracking has been performed using the Xsuite software package [18], a novel Python-based software that reimplements and extends the SixTrack single-particle code [19] following modern programming paradigms and allowing efficient GPU parallelisation. The code structure allowed us to easily implement in the particle tracking the normalisation of shadow particles for every turn tracked, and it made it possible to track a large amount of initial conditions thanks to the computing possibilities offered by GPUs. For both models, the initial conditions were sampled on a regular  $100 \times 100$   $2d$  Cartesian grid in the transverse

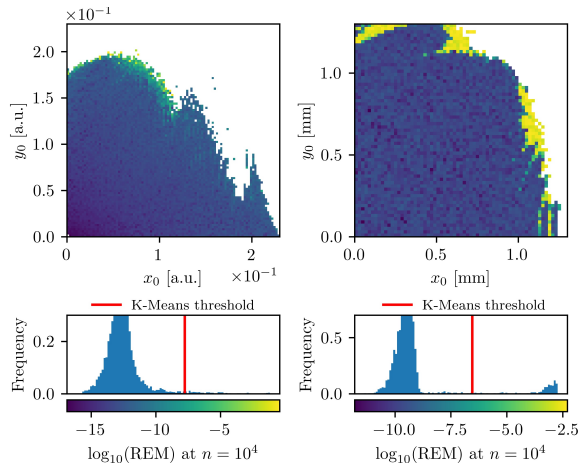


Figure 2: REM computed at  $n = 10^4$  for the Hénon map (left) and the HL-LHC lattice (right). The shape of the REM distribution enables efficient K-Means clustering.

$x - y$  plane, with initial  $p_x = p_y = 0$ , and for the HL-LHC model, the longitudinal variables were set to zero.

To test the predictive power of chaos detection by dynamic indicators, we define and perform a Ground Truth (GT) classification based on FLI calculated for  $n_{\max} = 10^8$  (Hénon map) or  $10^7$  (HL-LHC lattice). The resulting distribution shows a main cluster of non-chaotic particles with a lower mean FLI value and a secondary cluster of chaotic particles with a higher mean FLI value. A K-Means algorithm [20] is used to compute a threshold to distinguish the two clusters. This threshold value is used for a binary chaotic/non-chaotic classification of initial conditions (see this entire process for both models in Fig. 1).

We define as predictive performance of a dynamic indicator the accuracy, i.e. the ratio between the correctly labelled initial conditions and the total number of initial conditions, achieved in the GT reconstruction, with the K-Means approach applied to the dynamic indicators computed for  $n < n_{\max}$ . A good dynamic indicator should achieve the correct identification of chaotic particles even when  $n \ll n_{\max}$ , allowing the correct clustering detection and binary classification based on the threshold computed with K-Means. Figure 2 shows an example of both models obtained with REM for  $n = 10^4$ . The threshold calculated by the K-Means algorithm is also displayed. The large separation between the two distributions of REM values for the HL-LHC case makes clustering easy.

Figure 3 compares the distribution of FLI and REM, for the HL-LHC. Their distributions follow a different evolution with  $n$ . Clustering might be particularly hard for FLI at low  $n$ , as its distributions do not feature a clear separation between the chaotic/non-chaotic components.

The accuracy achieved by all dynamic indicators considered as a function of  $n$  is shown in Fig. 4. For both models, Lyapunov-based dynamic indicators exhibit a marked step-like increase in performance for  $n$  3-4 orders of magnitude lower than  $n_{\max}$ , followed by a steady increase as  $n$

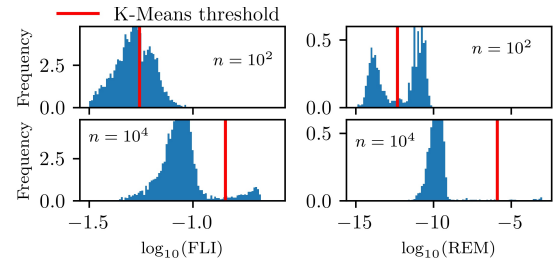


Figure 3: Histograms of FLI and REM for HL-LHC. FLI does not show the presence of a second cluster at  $n = 10^2$  so that it can be classified correctly by K-Means. REM generates a secondary cluster already at  $n = 10^2$ .

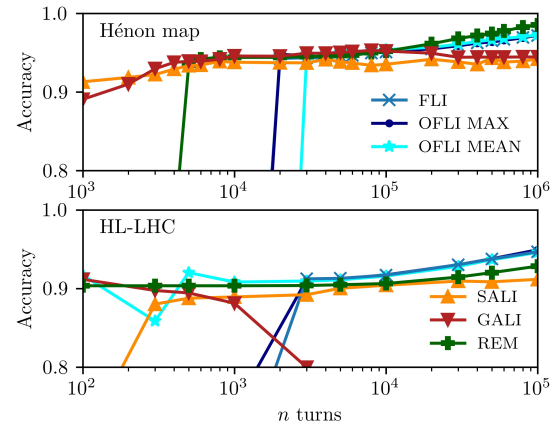


Figure 4: Accuracy achieved by the dynamic indicators at reconstructing the GT.

approaches  $n_{\max}/100$ . This step-like increase is related to the time needed by the dynamic indicators to reach a value distribution that is approachable with K-Means clustering. SALI and GALI, instead, feature a better performance for very low  $n$ , but then remains constant over the time interval explored, with the exception of GALI showing a decreasing performance for HL-LHC.

## CONCLUSIONS AND OUTLOOK

An exploratory study of dynamic indicators was carried out on accelerator-related models to test the performance in predicting chaotic behaviour. Chaos detection is performed in combination with a K-Means algorithm used as a clustering strategy for the distribution of the dynamic indicator. The performance of a dynamic indicator is provided by reconstructing a Ground Truth computed at a high number of turns. The results are rather similar for the two models and indicate that REM, SALI, and GALI may provide a better and early detection of chaos compared to Lyapunov-based indicators. However, these show a steady improvement with the number of turns  $n$ .

Future research will address the confirmation of these results in more models and the testing of more refined clustering strategies to fully exploit the predictive potential of dynamic indicators. Moreover, the analysis should be extended to  $6d$ , also including longitudinal dynamics.

## REFERENCES

- [1] M. Giovannozzi, W. Scandale, and E. Todesco, "Dynamic aperture extrapolation in the presence of tune modulation," *Physical Review E*, vol. 57, no. 3, p. 3432, 1998, doi:10.1103/PhysRevE.57.3432
- [2] A. Bazzani, G. Servizi, G. Turchetti, and E. Todesco, *A normal form approach to the theory of nonlinear betatronic motion*. CERN, 1994.
- [3] I. Béjar Alonso, O. Brüning, P. Fessia, L. Rossi, L. Tavian, and M. Zerlauth, *High-Luminosity Large Hadron Collider (HL-LHC): Technical design report*, I. Béjar Alonso, Ed. CERN, 2020, doi:10.23731/CYRM-2020-0010
- [4] F. Panichi, L. Ciotti, and G. Turchetti, "Fidelity and reversibility in the restricted three body problem," *Communications in Nonlinear Science and Numerical Simulation*, vol. 35, pp. 53–68, 2016, doi:10.1016/j.cnsns.2015.10.016
- [5] F. Panichi, K. Goździewski, and G. Turchetti, "The reversibility error method (REM): a new, dynamical fast indicator for planetary dynamics," *Monthly Notices of the Royal Astronomical Society*, vol. 468, no. 1, pp. 469–491, 2017, doi:10.1093/mnras/stx374
- [6] E. Lega, M. Guzzo, and C. Froeschlé, "Theory and Applications of the Fast Lyapunov Indicator (FLI) Method," in *Chaos Detection and Predictability*. 2016, pp. 35–54, doi:10.1007/978-3-662-48410-4\_2
- [7] E. Todesco, M. Giovannozzi, and W. Scandale, "Fast indicators of long-term stability," *Part. Accel.*, vol. 55, pp. 27–36, 1996, <https://cds.cern.ch/record/316950>
- [8] Y. Li, Y. Hao, K. Hwang, R. Rainer, A. He, and A. Liu, "Fast dynamic aperture optimization with forward-reversal integration," *Nuclear Instruments and Methods in Physics Research Section A: Accelerators, Spectrometers, Detectors and Associated Equipment*, vol. 988, p. 164936, 2021, doi:10.1016/j.nima.2020.164936
- [9] C. Skokos and T. Manos, "The Smaller (SALI) and the Generalized (GALI) Alignment Indices: Efficient Methods of Chaos Detection," in *Chaos Detection and Predictability*. 2016, pp. 129–181, doi:10.1007/978-3-662-48410-4\_5
- [10] C. Skokos, "The Lyapunov Characteristic Exponents and Their Computation," in *Dynamics of Small Solar System Bodies and Exoplanets*. 2010, pp. 63–135, doi:10.1007/978-3-642-04458-8\_2
- [11] R. Barrio, W. Borczyk, and S. Breiter, "Spurious structures in chaos indicators maps," *Chaos, Solitons & Fractals*, vol. 40, no. 4, pp. 1697–1714, 2009, doi:10.1016/j.chaos.2007.09.084
- [12] G. Turchetti and F. Panichi, "Fast Indicators for Orbital Stability: A Survey on Lyapunov and Reversibility Errors," in *Progress in Relativity*, 2019, ch. 10, doi:10.5772/intechopen.88085
- [13] R. Barrio, "Theory and Applications of the Orthogonal Fast Lyapunov Indicator (OFLI and OFLI2) Methods," in *Chaos Detection and Predictability*. 2016, pp. 55–92, doi:10.1007/978-3-662-48410-4\_3
- [14] "IEEE Standard for Floating-Point Arithmetic," *IEEE Std 754-2019 (Revision of IEEE 754-2008)*, pp. 1–84, 2019, doi:10.1109/IEEESTD.2019.8766229
- [15] C. Skokos, "Alignment indices: A new, simple method for determining the ordered or chaotic nature of orbits," *Journal of Physics A: Mathematical and General*, vol. 34, no. 47, pp. 10029–10043, 2001, doi:10.1088/0305-4470/34/47/309
- [16] C. Skokos, T. Bountis, and C. Antonopoulos, "Geometrical properties of local dynamics in hamiltonian systems: The generalized alignment index (gali) method," *Physica D: Nonlinear Phenomena*, vol. 231, no. 1, pp. 30–54, 2007, doi:10.1016/j.physd.2007.04.004
- [17] E. Todesco and M. Giovannozzi, "Dynamic aperture estimates and phase-space distortions in nonlinear betatron motion," *Physical Review E*, vol. 53, no. 4, p. 4067, 1996, doi:10.1103/PhysRevE.53.4067
- [18] G. Iadarola. "Xsuite documentation pages.", 2022. <https://xsuite.readthedocs.io>
- [19] R. D. Maria *et al.*, "SixTrack version 5: Status and new developments," *Journal of Physics: Conference Series*, vol. 1350, no. 1, p. 012129, 2019, doi:10.1088/1742-6596/1350/1/012129
- [20] H.-H. Bock, "Clustering methods: A history of k-means algorithms," in *Selected Contributions in Data Analysis and Classification*. 2007, pp. 161–172, doi:10.1007/978-3-540-73560-1\_15